Computational Study of Scission Neutrons in Low-Energy Fission: Stationary and Time-Dependent Approaches

M. Rizea[1,*] and N. Carjan[1,2]

[1] *National Institute of Physics and Nuclear Engineering, "Horia Hulubei",*
PO Box MG-6, Bucharest, Romania.
[2] *Centre d'Etudes Nucléaires de Bordeaux-Gradignan, UMR 5797,*
CNRS/ IN2P3-Université Bordeaux 1, BP 120, 33175 Gradignan Cedex, France.

Abstract. The emission of scission neutrons from fissioning nuclei is of high practical interest. To study this process we have used the sudden approximation and also a more realistic approach that takes into account the scission dynamics. Numerically, this implies the solution of the bi-dimensional Schrödinger equation, both stationary and time-dependent. To describe axially symmetric extremely deformed nuclear shapes, we have used the Cassini parametrization. The Hamiltonian is discretized by using finite difference approximations of the derivatives. The main computational challenges are the solution of algebraic eigenvalue problems and of linear systems with large sparse matrices. We have employed appropriate procedures (Arnoldi and bi-conjugate gradients). The numerical solutions have been used to evaluate physical quantities, like the number of emitted neutrons per scission event, the primary fragments' excitation energy and the distribution of the emission points.

1 Introduction

During the last years, there has been an increasing interest in the simulation of fundamental processes in quantum systems by numerical methods. In this context, the solution of the Schrödinger equation plays a major role in the investigation of phenomena

---

*Corresponding author. *Email addresses:* `rizea@theory.nipne.ro` (M. Rizea), `carjan@cenbg.in2p3.fr` (N. Carjan)

like nuclear fission and fusion, atomic and nuclear collisions, laser-atom interaction. In the present paper we focus on the scission neutrons, subject of present interest, important for nuclear applications. Among the neutrons emitted during fission, one can distinguish chronologically three categories: the scission neutrons (10^{-21}-10^{-20} s), the prompt neutrons (10^{-18}-10^{-16} s) and the delayed neutrons ($> 10^{-16}$ s). The last two components form the large majority of fission neutrons and have been extensively studied. The scission neutrons were less investigated, but are recently receiving an increasing attention. Estimated to represent 10-30% of the total number of neutrons, this kind of neutrons are considered responsible for important effects observed in the fission process (see [1–7]) and are essential ingredients in numerical reactor simulations. One possible approach to study the emission of scission neutrons is the sudden approximation [8]. This implies the numerical solution of an eigenvalue problem associated to the bi-dimensional stationary Schrödinger equation for independent neutrons in axially symmetric extremely deformed nuclear shapes. We have used a grid-based procedure, in which the equation is discretized by finite difference approximations of the derivatives. We are led to an algebraic eigenvalue problem with large (sparse) matrix, which is solved by the Implicitly Restarted Method of Arnoldi. In the sudden approximation the scission is seen as a sudden transition between two different nuclear configurations. By calculating the bound state wavefunctions just-before-scission (ϵ_i) and immediately-after-scission (ϵ_f), one can evaluate physical quantities like: the number of scission neutrons per fission event and the excitation energy of primary fission fragments. An alternative approach is to consider the last stage of the fission process as a time dependent fast (diabatic) process. By solving the bi-dimensional time-dependent Schrödinger equation (TDSE) with a potential variable in time between ϵ_i and ϵ_f, one can study the scission process in a more realistic model. The numerical solution of TDSE is obtained by a Crank-Nicolson scheme, which requires the solution of large sparse linear systems that was obtained by a variant of the bi-conjugate gradient method. Transparent Boundary Conditions have been implemented, to avoid reflexions on the numerical boundaries.

A similar time-dependent approach was applied in [9] to a different sequence of nuclear shapes during fission, namely to the descent of the fissioning nucleus from the saddle point to the scission point. The numerical calculation capabilities being quite limited at that time, the authors had to neglect the spin-orbit coupling, use a non-diffuse nuclear potential (square well) and a much smaller spatio-temporal grid.

In the following we present some details on the physical problem, on the mathematical model and on the numerical procedures. Also, some results in a definite case will be shown.

2   The bi-dimensional Schrödinger equation

To obtain the bound states, one has to solve the eigenvalue problem:

$$\mathcal{H}\Psi = E\Psi, \tag{2.1}$$

with appropriate boundary conditions. $\mathcal{H}$ is the Hamiltonian, which includes the Laplacean, the nuclear potential, the spin-orbit coupling and, for charged particles, the Coulomb potential. The nuclear shape is assumed to be axially symmetric and we use cylindrical coordinates.

The total wavefunction has two components, corresponding to spin-up and spin-down as follows

$$\Psi(\rho,z,\phi) = f_1(\rho,z)e^{i\Lambda_1\phi}|\uparrow\rangle + f_2(\rho,z)e^{i\Lambda_2\phi}|\downarrow\rangle, \tag{2.2a}$$

$$\Lambda_1 = \Omega - \frac{1}{2}, \qquad \Lambda_2 = \Omega + \frac{1}{2}. \tag{2.2b}$$

Ω is the projection of the total angular momentum along the symmetry axis. Due to the axial symmetry, the angular dependence is removed and the equation $\mathcal{H}\Psi = E\Psi$ can be written as:

$$\begin{bmatrix} O_1 - KS_c & -KS_a \\ -KS_b & O_2 - KS_d \end{bmatrix} \begin{bmatrix} f_1 \\ f_2 \end{bmatrix} = E \begin{bmatrix} f_1 \\ f_2 \end{bmatrix}. \tag{2.3}$$

The operators O_1, O_2 contain the Laplacean:

$$O_{1,2} = -\frac{\hbar^2}{2\mu}\left(\Delta - \frac{\Lambda_{1,2}^2}{\rho^2}\right) + V(\rho,z), \qquad \Delta = \frac{1}{\rho}\frac{\partial}{\partial\rho} + \frac{\partial^2}{\partial\rho^2} + \frac{\partial^2}{\partial z^2}.$$

$\hbar$ is the Planck constant, μ is the reduced mass, $V(\rho,z)$ is the potential, K is a constant and

$$S_a = \frac{\partial V}{\partial\rho}\frac{\partial}{\partial z} - \frac{\partial V}{\partial z}\left(\frac{\partial}{\partial\rho} + \frac{\Lambda_2}{\rho}\right), \qquad S_b = -\frac{\partial V}{\partial\rho}\frac{\partial}{\partial z} + \frac{\partial V}{\partial z}\left(\frac{\partial}{\partial\rho} - \frac{\Lambda_1}{\rho}\right),$$

$$S_c = \frac{\partial V}{\partial\rho}\frac{\Lambda_1}{\rho}, \qquad\qquad\qquad S_d = -\frac{\partial V}{\partial\rho}\frac{\Lambda_2}{\rho}.$$

The operators $S_a, \cdots, S_d$ represent the spin-orbit coupling.

Let us note that the Hamiltonian can be simplified by the transformations $g_1 = \rho^{1/2}f_1, g_2 = \rho^{1/2}f_2$, which remove the first derivative from the Laplacean operator. It results a new Hamiltonian $\hat{\mathcal{H}}$ which has the same eigenvalues as $\mathcal{H}$ and its eigenfunctions are the pairs g_1, g_2, related to f_1, f_2 by the above mentioned transformation. The Hamiltonian $\hat{\mathcal{H}}$ is self-adjoint for null boundary conditions (corresponding to bound states), so that its spectrum is real (see [10]). With the notations:

$$L_1 = -\frac{\hbar^2}{2\mu}\left(\frac{\partial^2}{\partial\rho^2} + \frac{\partial^2}{\partial z^2} + \frac{1/4 - \Lambda_1^2}{\rho^2}\right) + V(\rho,z), \tag{2.4a}$$

$$L_2 = -\frac{\hbar^2}{2\mu}\left(\frac{\partial^2}{\partial\rho^2} + \frac{\partial^2}{\partial z^2} + \frac{1/4 - \Lambda_2^2}{\rho^2}\right) + V(\rho,z), \tag{2.4b}$$

$$Q_1 = K\left(\frac{\partial V}{\partial\rho}\frac{\partial}{\partial z} - \frac{\partial V}{\partial z}\frac{\partial}{\partial\rho}\right), \qquad Q_2 = K\frac{\Omega}{\rho}\frac{\partial V}{\partial z}, \tag{2.4c}$$

$$P_a = -Q_1 + Q_2, \quad P_b = Q_1 + Q_2, \quad P_c = -K\frac{\Lambda_1}{\rho}\frac{\partial V}{\partial\rho}, \quad P_d = K\frac{\Lambda_2}{\rho}\frac{\partial V}{\partial\rho}, \tag{2.4d}$$

the eigenvalue problem for the Hamiltonian $\hat{\mathcal{H}}$ can be written in the form:

$$\begin{bmatrix} L_1+P_c & P_a \\ P_b & L_2+P_d \end{bmatrix} \begin{bmatrix} g_1 \\ g_2 \end{bmatrix} = E \begin{bmatrix} g_1 \\ g_2 \end{bmatrix}. \tag{2.5}$$

2.1 Nuclear shape description

To describe the nuclear shape we have used the Cassini parametrization, appropriate for strong deformations, as appearing during the nuclear fission. The Cassinian ovals are taken as the first approximation to the nuclear shape and the deviation from it is represented by a Legendre polynomial expansion. In the Cassini parametrization (see [11,12]) an axially deformed shape is described in cylindrical coordinates by the relations:

$$\bar{\rho} = \frac{1}{\sqrt{2}} \left(Q(x) - R^2(x)(2x^2-1) - s \right)^{\frac{1}{2}}, \tag{2.6a}$$

$$\bar{z} = \frac{\text{sign}(x)}{\sqrt{2}} \left(Q(x) + R^2(x)(2x^2-1) + s \right)^{\frac{1}{2}}, \tag{2.6b}$$

where

$$Q(x) = \left(R^4(x) + 2sR^2(x)(2x^2-1) + s^2 \right)^{\frac{1}{2}},$$

$s = \epsilon R_0^2$ is the squared distance from the focus of Cassinian ovals to the origin and $-1 \leq x \leq 1$. The function $R(x)$ is given in terms of Legendre polynomials by:

$$R(x) = R_0 \left(1 + \sum \alpha_m P_m(x) \right), \quad m \geq 1.$$

The set of parameters (ϵ, α_m) determines the nuclear shape. In practice, the following transformations are performed:

$$\bar{\rho} = c\rho, \qquad \bar{z} = cz + \bar{z}_m.$$

c is determined by the requirement that the volume enclosed by the surface is constant, independent of nuclear deformation (expressing the incompressibility of nuclear matter), while $\bar{z}_m$ results by fixing the center of mass at the origin.

2.2 The definition of the potential

To define the potential, we consider the function

$$\Phi(\rho, z) = \left((z^2 + \rho^2)^2 - 2\epsilon R_0^2 (z^2 - \rho^2) + \epsilon^2 R_0^4 \right)^{\frac{1}{4}} - R_0 \left(1 + \sum_{m \geq 1} \alpha_m P_m(x) \right).$$

The equation $\Phi(\rho,z) = 0$ represents the nuclear surface in cylindrical coordinates. The nuclear potential is given by

$$V(\rho,z) = -V_0 \left[1 + \exp\left(\frac{\Theta}{a_0}\right)\right]^{-1}, \tag{2.7}$$

where V_0 is the depth and a_0 the diffuseness. The quantity Θ is an approximation to the distance between the point (ρ,z) and the nuclear surface, given by the expression: $\Theta(\rho,z) = \Phi/|\nabla\Phi|$ (see [12]). At $\epsilon = 0$, the potential (2.7) turns into the Woods-Saxon potential of the spherical nucleus.

The spin-orbit interaction is taken proportional to the gradient of the potential (2.7):

$$V_{so} = -K[\bar{\sigma} \times \bar{p}]\nabla V, \qquad K = \lambda\left(\frac{\hbar}{2\mu c}\right)^2, \tag{2.8}$$

where $\bar{\sigma}$ and $\bar{p}$ are the nucleon spin and momentum (see [13]). The constant K depends on the Compton wavelength and on the parameter λ. Transforming to cylindrical coordinates (ρ,z,ϕ) and using the assumed axial symmetry in the form $\partial V/\partial\phi = 0$, we find

$$V_{so} = -\left(\frac{K}{2}\right)S,$$

$$S = \sigma^+ e^{-i\phi}\left\{\frac{\partial V}{\partial\rho}\frac{\partial}{\partial z} - \frac{\partial V}{\partial z}\left[\frac{\partial}{\partial\rho} + \frac{1}{\rho}\left(-i\frac{\partial}{\partial\phi}\right)\right]\right\} + \sigma^- e^{i\phi}\left\{-\frac{\partial V}{\partial\rho}\frac{\partial}{\partial z}\right.$$

$$\left. + \frac{\partial V}{\partial z}\left[\frac{\partial}{\partial\rho} - \frac{1}{\rho}\left(-i\frac{\partial}{\partial\phi}\right)\right]\right\} + 2\sigma_z\frac{\partial V}{\partial\rho}\frac{1}{\rho}\left(-i\frac{\partial}{\partial\phi}\right).$$

Here $\sigma^{\pm} = \sigma_x \pm i\sigma_y$ and $\sigma_x, \sigma_y, \sigma_z$ are the Pauli matrices:

$$\sigma_x = \begin{pmatrix} 0 & 1 \\ 1 & 0 \end{pmatrix}, \quad \sigma_y = \begin{pmatrix} 0 & -i \\ i & 0 \end{pmatrix}, \quad \sigma_z = \begin{pmatrix} 1 & 0 \\ 0 & -1 \end{pmatrix}.$$

Applied to functions of the mentioned form (up+down) this V_{so} gives rise to the additional terms $S_a, \cdots, S_d$ in Eq. (2.3).

Note that all the components of the resulting Hamiltonian are real and the wavefunction is defined in terms of the real functions f_1 and f_2. As mentioned, this Hamiltonian can be simplified, leading to wavefunctions with the components g_1 and g_2, also real.

For charged particles, the potential contains also a Coulomb term (see [12]).

3   The computational model

For numerical treatment, the infinite physical domain is reduced to a finite one, $[0,R] \times [-Z,Z]$, which is discretized by a grid with the mesh points:

$$\rho_j = j\Delta\rho, \quad j = 1, \cdots, N_\rho, \qquad z_k = k\Delta z, \quad k = -N_z, \cdots, N_z. \tag{3.1}$$

For $j=N_\rho$, $\rho_j=R$ and for $k=N_z$, $z_k=Z$. The axis $\rho=0$ is excluded since on it the wave function (with the components g_1 and g_2) is assumed to be zero. At each point the partial derivatives appearing in $\hat{\mathcal{H}}$ are approximated by finite difference formulae. But these formulae should correspond to the behavior of the solution. Instead of standard formulae, in the vicinity of $\rho=0$ we shall use adapted formulae, which take into account the operated function transformation (of the form $g=\rho^{1/2}f$). To introduce them, let us consider the one-dimensional eigenvalue problem on the interval $[0,1]$:

$$-\Delta f + \frac{\Lambda^2}{\rho^2}f = Ef, \tag{3.2}$$

with the boundary conditions: $f'(0)=0$ (for $\Lambda \neq 1$) or $f(0)=0$ (for $\Lambda=1$) and $f(1)=0$. Λ is a nonnegative integer and Δ is the Laplacean in polar coordinates defined by

$$\Delta f = \frac{d^2 f}{d\rho^2} + \frac{1}{\rho}\frac{df}{d\rho}, \tag{3.3}$$

where f is a cylindrically symmetric function of ρ.

By the transformation $g(\rho) \equiv \rho^{1/2} f(\rho)$, Eq. (3.2) is modified as follows:

$$-\frac{d^2 g}{d\rho^2} + \frac{\Lambda^2 - 1/4}{\rho^2}g = Eg. \tag{3.4}$$

The above transformation is in fact the Liouville transformation, applied to that particular equation. It eliminates the first derivative and modifies the scalar product from $\int_0^\infty f_m^* f_n \rho \, d\rho$ to the simpler expression $\int_0^\infty g_m^* g_n \, d\rho$. The boundary conditions can now be rewritten as: $g(0)=g(1)=0$. The condition $g(0)=0$ is fulfilled provided that $f(0)$ is finite and this is ensured by the conditions for f.

It is known that the equation

$$w'' + \left(\kappa^2 - \frac{\Lambda^2 - 1/4}{\rho^2}\right)w = 0 \tag{3.5}$$

has as regular solution $w = \rho^{1/2} J_\Lambda(\kappa\rho)$, where J_Λ is the Bessel function of the first kind (see [14], Eq. (9.1.49)). Since $w(1)=J_\Lambda(\kappa)$, if κ is a zero of J, $w(1)=0$ and the solution of our eigenvalue problem is $g(\rho)=\rho^{1/2}J_\Lambda(\kappa\rho)$ and the eigenvalue is $E=\kappa^2$.

Now, we want to solve numerically the problem associated to Eq. (3.4) by approximating the derivative through finite differences, which converts the differential problem into an algebraic eigenvalue problem. Let us consider a partition of the $[0,1]$ interval with the mesh points $\rho_j = jh$, $j=0,\cdots,J$, $\rho_J=1$. The standard finite difference approximation of the second derivative is

$$g_j'' \approx \frac{g_{j+1} - 2g_j + g_{j-1}}{h^2}, \tag{3.6}$$

where $g_j = g(jh)$. This formula is exact for polynomials up to some degree (the leading term of the error is proportional to $g^{(4)}$). It is appropriate for the function f from Eq. (3.2),

which has a normal Taylor expansion around $\rho = 0$. But the function g, which is the product of f by the factor $\rho^{1/2}$, has a different behavior. In fact, the regular solution of Eq. (3.4) is of the form:

$$g(\rho) = \rho^{\frac{1}{2}+\Lambda} \sum_{i=0}^{\infty} \alpha_{2i}\rho^{2i}. \tag{3.7}$$

We look for a difference formula adapted to such a function. We shall take it of the form:

$$g''_j \approx \frac{a_j g_{j+1} + b_j g_j + a_j g_{j-1}}{h^2}. \tag{3.8}$$

The coefficients a_j, b_j are determined so that the formula is exact when g is replaced by $\rho^{1/2+\Lambda}$ and $\rho^{5/2+\Lambda}$ (the leading terms of the expansion). It results:

$$a_j = \frac{4(\Lambda+1)}{j^2(p_j - q_j)}, \qquad\qquad b_j = \frac{1}{j^2}\left[\Lambda^2 - \frac{1}{4} - \frac{4(\Lambda+1)q_j}{p_j - q_j}\right], \tag{3.9a}$$

$$p_j = \left(1+\frac{1}{j}\right)^{\Lambda+\frac{5}{2}} + \left(1-\frac{1}{j}\right)^{\Lambda+\frac{5}{2}}, \qquad q_j = \left(1+\frac{1}{j}\right)^{\Lambda+\frac{1}{2}} + \left(1-\frac{1}{j}\right)^{\Lambda+\frac{1}{2}}. \tag{3.9b}$$

Note that $a_j \rightarrow 1$, $b_j \rightarrow -2$, as $j \rightarrow \infty$, i.e., the formula (3.8) approaches the standard one with increasing j.

Using the formula (3.8) in Eq. (3.5), we obtain the following algebraic eigenvalue problem (E is the eigenvalue and g_j form the eigenvector):

$$-\frac{a_j g_{j+1} + b_j g_j + a_j g_{j-1}}{h^2} + \frac{\Lambda^2 - 1/4}{\rho_j^2} g_j = E g_j, \quad j = 1, \cdots, J-1, \ \ g_0 = g_J = 0. \tag{3.10}$$

This problem has been solved with the package ARPACK [15], based on the Implicitly Restarted Method of Arnoldi.

To show the effect of the modification in the finite difference formula, we present in the Table 1 some results with both formulae: standard and adapted. For $\Lambda = 0$, the errors in the first three eigenvalues at different step sizes are given.

One can see a clear gain in accuracy with the adapted formula, especially for the first eigenvalue. An even better adapted formula can be obtained if we ask it to be also satisfied by the next terms in the expansion (3.7), but then the formula must contain more variable coefficients (see [10]).

For $\Lambda > 0$, the difference between the adapted formula and the standard one is smaller, since the polynomial component of the solution becomes more important (its leading term is $\rho^{\Lambda+1/2}$), but still the adapted formula is superior. We should mention that the variable coefficient is used only near $\rho = 0$, where the particular behavior of g is dominant. In the rest of the interval, the standard formula is applied. An appropriate switching point is $\rho = 0.25$, as found by numerical experiments.

In conclusion, the transformation $g = \sqrt{\rho}f$ simplifies the equation, eliminating the needs of an additional approximation, namely of the first derivative. Also, the treatment

Table 1: Comparison of the standard (S) and adapted (A) finite difference formulae at $\Lambda = 0$.

h	E_{exact}	$E_{calc}(S)$	$E_{calc}(A)$	$Rel.er(S)$	$Rel.er(A)$
$\frac{1}{32}$	5.78319	7.21109	5.78289	2.47E-01	5.05E-05
	30.4713	34.1084	30.3983	1.19E-01	2.40E-03
	74.8870	80.6720	74.4383	7.72E-02	5.99E-03
$\frac{1}{64}$	5.78319	7.04874	5.78316	2.19E-01	4.04E-06
	30.4713	33.7193	30.4530	1.07E-01	6.00E-04
	74.8870	80.2693	74.7741	7.19E-02	1.51E-03
$\frac{1}{128}$	5.78319	6.91703	5.78319	1.96E-01	1.56E-07
	30.4713	33.3679	30.4667	9.51E-02	1.50E-04
	74.8870	79.7173	74.8587	6.45E-02	3.77E-04

of the point $\rho = 0$ is easier. When $\Lambda \neq 0$, the equation in f contains a singular term (Λ^2/ρ^2) and thus the origin should be avoided in the discretization and the value of $f(0)$ cannot be obtained. Conversely, $g(0) = 0$, so that only the values g_j, $j \geq 1$ have to be calculated. The scalar product, of the form $\int g_m^* g_n d\rho$, can be conveniently evaluated-no special procedure near the origin is required. So, in practice it is more advantageous to deal with the transformed equation, but the finite differences used in the discretization should be adapted to the induced behavior of the solution.

We implemented this experience in the discretization of the Hamiltonian in two dimensions. For the derivatives in ρ we have used adapted formulae, while the derivatives with respect to z are approximated by standard formulae. Note that, however, the Hamiltonian $\hat{\mathcal{H}}$ still contain first derivatives with respect to ρ (the Liouville transformation removes the derivatives only in the Laplacean part). These derivatives are approximated as well by adapted difference formulae, deduced likewise as those for second order derivatives. We have used the following formula, exact for the functions $\rho^{\Lambda+1/2}$ and $\rho^{\Lambda+5/2}$:

$$g_j' \approx \frac{d_j g_{j+1} + e_j g_j - d_j g_{j-1}}{h}, \tag{3.11}$$

where

$$d_j = \frac{2}{j(v_j - u_j)}, \qquad e_j = \frac{1}{j}\left(\Lambda + \frac{1}{2} - \frac{2u_j}{v_j - u_j}\right),$$

with

$$v_j = \left(1 + \frac{1}{j}\right)^{\Lambda + \frac{5}{2}} - \left(1 - \frac{1}{j}\right)^{\Lambda + \frac{5}{2}}, \qquad u_j = \left(1 + \frac{1}{j}\right)^{\Lambda + \frac{1}{2}} - \left(1 - \frac{1}{j}\right)^{\Lambda + \frac{1}{2}}.$$

Note that $d_j \to 1/2$, $e_j \to 0$, as $j \to \infty$, i.e., the formula (3.11) approaches the standard one. When these adapted formulae are applied in the Hamiltonian $\hat{\mathcal{H}}$ approximation, one should use $\Lambda = \Lambda_1$ for g_1 and $\Lambda = \Lambda_2$ for g_2.

By discretization, the original eigenvalue problem is transformed to an algebraic eigenvalue problem, whose eigenvector is formed by the values of g_1 and g_2 at nodes. The matrix is sparse and contains the coefficients of derivative approximations, as well as the potential values at the mesh points. Its order is two times the number of nodes (at each point the solution has two components) and is usually large. To solve the resulting eigenvalue problem (of the form $Ax = \lambda x$) we have used the package ARPACK (see [15]) based on the Implicitly Restarted Arnoldi Method. It is able to efficiently find selected eigenpairs of a large sparse matrix. Thus only the portion of the spectrum with physical relevance is calculated. An important feature is that only the matrix-vector product Ax is needed. Hence, the matrix A should not be generated nor stored, which is a great advantage in computation, saving time and memory. The method is appropriate either for symmetric or nonsymmetric matrices, both for normal and generalized eigenvalue problem. Note that the matrix resulting by the discretization of $\hat{\mathcal{H}}$ is nonsymmetric, because of the finite difference approximation of the first derivatives. Its eigenvalues, calculated with the corresponding set from ARPACK, are however real, approximations of the true eigenvalues of the original Hamiltonian, which is self-adjoint for bound state conditions.

Let us note that the solution of the bi-dimensional stationary Schrödinger equation is also possible by other approaches, like the diagonalization in a complete basis (see, e.g., [8]), but the grid-based procedure with finite differences, in spite of requiring longer computer time, exhibits certain advantages. Among them, we mention the convenient and uniform treatment of any nuclear shapes, symmetric as well as non-symmetric and the possibility to use the same numerical approximations in the solution of the time-dependent Schrödinger equation, which ensures compatible initial wave functions (in the evolutive model they are eigensolutions of the stationary equation with a potential $V(\rho,z)$ for which deformation parameters correspond to the pre-scission nuclear shape) and accurate propagated solutions.

3.1 Solution of the eigenvalue problem

The Arnoldi procedure combines some features of QR and power methods and constructs eigenpairs of the large matrix A from the eigenpairs of a small matrix H. The power method begins with a random vector v_0 and constructs a sequence of vectors $v_i = Av_{i-1} = A^i v_0$. Let us consider the space generated by the vectors $v_0, Av_0, \cdots, A^{k-1} v_0$ (i.e., the set of linear combinations). We call it the k'th Krylov subspace and will denote it by $\mathcal{K}_k(A, v_0)$. We define a Ritz pair as a pair (x_i, λ_i) that satisfies the Galerkin condition:

$$v^T(Ax_i - \lambda_i x_i) = 0, \qquad \forall v \in \mathcal{K}_k(A, v_0).$$

The k-step Arnoldi factorization of $A \in \mathbf{C}^{n \times n}$ is a relation of the form:

$$AV = VH + f e_k^T,$$

where $V \in \mathbf{C}^{n \times k}$ has orthonormal columns, $V^H f = 0$, $H \in \mathbf{C}^{k \times k}$ is upper Hessenberg with a non-negative subdiagonal and $\{e_j\}_{j=1}^n$ is the standard basis set for $\mathbf{C}^n$.

If $(\boldsymbol{y},\lambda)$ is an eigenpair of $\boldsymbol{H}$, since $\boldsymbol{V}^H\boldsymbol{f}=0$, it easily follows that λ is a Ritz value and $\boldsymbol{x}=\boldsymbol{V}\boldsymbol{y}$ a corresponding Ritz vector. We assume that $k\ll n$ so that the eigenpairs of $\boldsymbol{H}$ can be computed by a conventional method.

Also, the following relation is satisfied:

$$\| \boldsymbol{A}\boldsymbol{x}-\boldsymbol{x}\lambda \|=\| \boldsymbol{A}\boldsymbol{V}\boldsymbol{y}-\boldsymbol{V}\boldsymbol{y}\lambda \|=\| (\boldsymbol{A}\boldsymbol{V}-\boldsymbol{V}\boldsymbol{H})\boldsymbol{y} \|=\| \boldsymbol{f}\boldsymbol{e}_k^T\boldsymbol{y} \|=\beta|\boldsymbol{e}_k^T\boldsymbol{y}|, \qquad (3.12)$$

where $\|\cdot\|$ means the Euclidean norm and $\beta=\|\boldsymbol{f}\|$.

The process makes $|\boldsymbol{e}_k^T\boldsymbol{y}|\to 0$, so that the Ritz pair $(\boldsymbol{x},\lambda)$ well approximates an eigenpair of $\boldsymbol{A}$. The Implicitly Restarted Arnoldi Method consists in a succession of Arnoldi factorizations and eigenvalue estimations using the QR method.

4   The scission neutrons investigation

4.1   Stationary approach

Firstly, we consider the scission as a sudden transition between two different nuclear configurations. Immediately-after-scission the neutrons are still characterized by their just-before-scission wave functions $|\Psi^i\rangle$ but find themselves in the newly created potential of their interaction with the separated fragments. Their wave functions become wave packets with few positive-energy components. The probability to populate such unbound states gives the emission probability of a neutron that before scission has occupied the state $|\Psi^i\rangle$:

$$P_{em}^i = \sum_{\substack{unbound \\ states}} |a_{if}|^2, \qquad (4.1a)$$

$$a_{if} = \langle\Psi^i|\Psi^f\rangle = 2\pi \int \left(f_1^i f_1^f + f_2^i f_2^f\right)\rho d\rho dz = 2\pi \int \left(g_1^i g_1^f + g_2^i g_2^f\right)d\rho dz. \qquad (4.1b)$$

$|\Psi^f\rangle$ are the immediately-after-scission eigenstates. From computational point of view it is more convenient to obtain the bound states than the continuum states. Therefore we have used:

$$P_{em}^i = 1 - \sum_{\substack{bound \\ states}} |a_{if}|^2. \qquad (4.2)$$

Summing over all occupied states one obtains the total number of scission neutrons per fission event

$$\nu_{sc} = 2\sum_i v_i^2 P_{em}^i. \qquad (4.3)$$

The factor of 2 is due to the spin degeneracy (there are 2 neutrons on each level, corresponding to spin-up and spin-down). v_i^2 is the ground-state occupation probability of $|\Psi^i\rangle$. To obtain it one can consider the neutrons either independent or pairing correlated.

In the first case $v_i^2 = 1$ if the eigenenergy e_i is below some limit $e_{\max}$ (around Fermi level) and 0 otherwise (a step function). In the second case

$$v_i^2 = \frac{1}{2}\left(1 - \frac{e_i - \lambda}{\sqrt{(e_i - \lambda)^2 + \Delta^2}}\right), \tag{4.4}$$

with the parameters Δ and λ deduced from the Bardeen-Cooper-Schrieffer (BCS) equations (see [16]):

$$\sum_{i=n-n_c}^{n+n_c} \left((e_i - \lambda)^2 + \Delta^2\right)^{-\frac{1}{2}} - 2\tilde{g}(\tilde{\lambda})\ln\left(\frac{2\eta}{\tilde{\Delta}}\right) = 0, \tag{4.5}$$

with the constraint that the particle number $N = 2\sum_i v_i^2$ is conserved ($n = N/2$). The two cutoff parameters n_c and η are connected by

$$2\eta = 2n_c / \tilde{g}(\tilde{\lambda}),$$

where $\tilde{g}(\tilde{\lambda})$ is the average level density at the Fermi energy. The smooth gap parameter

$$\tilde{\Delta} = 13.3/\sqrt{A} \text{ MeV}$$

was taken from the systematics of odd-even mass differences in nuclei throughout the periodic table (see [17]).

Using the eigenstates, other characteristics of the process can be obtained, as the primary fragments' excitation energy and the spatial distribution of the emission points. Thus, the energy showing the degree of excitation in which the fragments are left is calculated from

$$E_{sc}^* = 2\sum_{\substack{bound \\ states}} (V_f^2 - v_f^2)e_f, \tag{4.6}$$

where

$$V_f^2 = \sum_i v_i^2 |a_{if}|^2 \tag{4.7}$$

is the occupation probability of the final state $|\Psi^f\rangle$ after the sudden transition and e_f is the corresponding eigenenergy.

The spatial distribution of the emission points is a function of the variables ρ and z given by:

$$S_{em}(\rho, z) = \sum_i v_i^2 |\Psi_{em}^i(\rho, z)|^2, \tag{4.8}$$

where

$$|\Psi_{em}^i\rangle = |\Psi^i\rangle - \sum_{\substack{bound \\ states}} a_{if}|\Psi^f\rangle \tag{4.9}$$

is the part of the initial wave function that has been emitted.

The numerical evaluation of integral in Eq. (4.1b) is performed by the Simpson formula. With respect to ρ the formula is adapted as well to the special form of the solutions g_1, g_2. Thus, close to $\rho = 0$ we have used the following formula with variable coefficients:

$$\frac{1}{2\Delta\rho} \int_{\rho_j}^{\rho_{j+2}} g(\rho)d\rho = \alpha_j g(\rho_j) + \beta_j g(\rho_{j+1}) + \alpha_j g(\rho_{j+2}). \tag{4.10}$$

The coefficients α_j, β_j result from the condition that the formula (4.10) is exact for the functions $\rho^{\Lambda+1/2}$ and $\rho^{\Lambda+5/2}$. We have obtained:

$$\alpha_j = \frac{\frac{1}{2\Lambda+7}\left[(j+2)^{\Lambda+\frac{7}{2}} - j^{\Lambda+\frac{7}{2}}\right] - \frac{(j+1)^2}{2\Lambda+3}\left[(j+2)^{\Lambda+\frac{3}{2}} - j^{\Lambda+\frac{3}{2}}\right]}{\left[(j+2)^{\Lambda+\frac{5}{2}} + j^{\Lambda+\frac{5}{2}}\right] - (j+1)^2\left[(j+2)^{\Lambda+\frac{1}{2}} + j^{\Lambda+\frac{1}{2}}\right]}, \tag{4.11a}$$

$$\beta_j = \frac{1}{2\Lambda+3} \frac{(j+2)^{\Lambda+\frac{3}{2}} - j^{\Lambda+\frac{3}{2}}}{(j+1)^{\Lambda+\frac{1}{2}}} - \alpha_j \frac{(j+2)^{\Lambda+\frac{1}{2}} + j^{\Lambda+\frac{1}{2}}}{(j+1)^{\Lambda+\frac{1}{2}}}. \tag{4.11b}$$

In the limit $j \to \infty$, these coefficients tend to the constant coefficients of the standard Simpson formula, i.e., $\alpha_j \to 1/6$ and $\beta_j \to 2/3$.

Before the calculation of the coefficients a_{if} (Eq. (4.1b)), the eigenfunctions provided by ARPACK are orthonormalized by the Gram-Schmidt algorithm in which the quadratures of the scalar product are done by the above described adapted Simpson formula.

We have applied the above formalism to study the emission of scission neutrons during the fission of ^{236}U. The numerical domain was: $\rho \in [\Delta\rho, 32]$, $z \in [-32, 32]$, while $\Delta\rho = \Delta z = 1/8$. Number of grid points: $N \approx 1.3 \times 10^5$. The two deformations between which the sudden transition is supposed to occur are characterized by the parameters $\epsilon_i = 0.985$ and $\epsilon_f = 1.001$ in the Cassini description of the nuclear shapes. The first value corresponds to a configuration with two fragments connected by a neck, while the second corresponds to separated fragments. The chosen values are in agreement with theoretical predictions for the minimum value of the neck radius (see [18]). The fission can be symmetric (each fragment has the mass 118) or, more frequently, asymmetric. As an example we present the case when one of the fragments has the mass $A_L = 86$. Depending of this mass and of ϵ one more deformation parameter (α_1) is obtained. It is adjusted such that the ratio of the volumes of the two fragments is equal to the ratio of the two masses A_H/A_L. An idea of the shapes involved is given by the equipotential lines corresponding to $V_0/2$, $V_0 = 40.22$ MeV being the depth of the nuclear potential (see Fig. 1, where the values of these parameters are also mentioned).

For $\Omega = 1/2$, there are 41 bound states for the initial configuration and 41 for the final one. For $\Omega = 3/2$ there are 27 states, 18 states for $\Omega = 5/2$, 9 states for $\Omega = 7/2$, 5 states for $\Omega = 9/2$ and 2 states for $\Omega = 11/2$. In the Table 2 we give the scission neutron multiplicity and the excitation energy (in MeV) at each Ω for the light fragment mass $A_L = 86$. For the occupation probabilities we have considered the particles independent (IP), in which case a step function is used and also correlated (PC), in which case the BCS parameters are used.
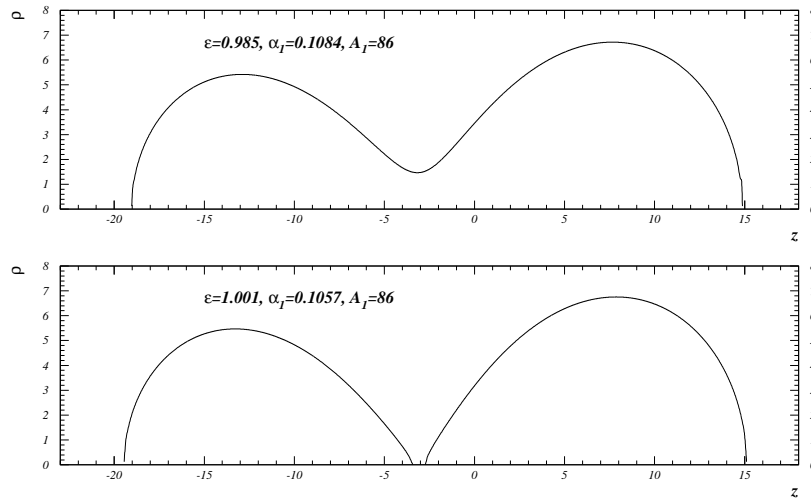
Figure 1: Equipotential lines corresponding to half of the depth of the nuclear potential at initial and final deformations.

Table 2: SN multiplicity and excitation energy for $A_L = 86$ at each Ω.

Ω	ν_{sc}-IP	ν_{sc}-PC	E_{sc}-IP	E_{sc}-PC
1/2	0.51734	0.47571	6.59002	3.00898
3/2	0.12290	0.14288	3.36928	2.91752
5/2	0.12235D-01	0.29941D-01	1.39202	2.24470
7/2	0.62626D-01	0.56349D-01	0.60892	1.25476
9/2	0.15587D-02	0.57264D-02	0.10724	1.50310
11/2	0.50968D-03	0.60584D-03	0.04671	0.13044
Sum	0.71716	0.71121	12.11418	11.05949

Table 3: SN multiplicity and excitation energy for $A_L = 86$, $\Omega = 5/2$.

$\Delta\rho, \Delta z$	ν_{sc}-IP	E_{sc}-IP
1/8	0.012235	1.39202
1/16	0.012223	1.39198

To verify the dependence of the results on the step size we have calculated for one case ($A_L = 86$, $\Omega = 5/2$ and Independent Particles probabilities) with a step size 2 times smaller ($\Delta\rho = \Delta z = 1/16$). The results are presented in the Table 3.

As one can see, the relative difference is less than 10^{-3}.

In Fig. 2 the spatial distributions of the emission points for $A_L = 86$ (mass asymmetry) and for $A_L = 118$ (mass symmetry) are shown (as functions of ρ and z, defined by Eq. (4.8)). The contributions from all Ω's between 1/2 and 11/2 have been taken into account. The BCS probability parameters have been used.
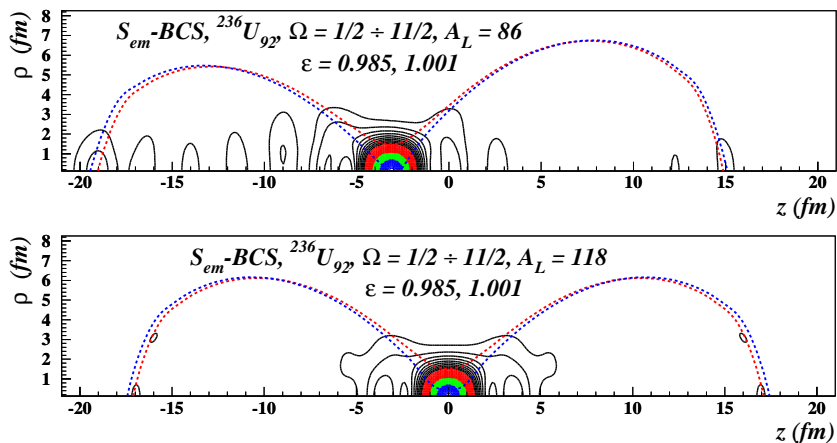
Figure 2: The distribution of the emission points at asymmetric ($A_L = 86$) and symmetric fission ($A_L = 118$).

In the used representation by contour lines, the dark regions correspond to the maximum values and one can see that the emission points are concentrated around the neck. To identify its place, we added in each figure the equipotential lines corresponding to $V_0/2$ before and after scission.

In fact, we have obtained the scission neutron multiplicity and the excitation energy for a set of light fragment masses A_L equally distributed in the range [70,118]. In the case of mass symmetry, the results have been compared with those corresponding to the wave
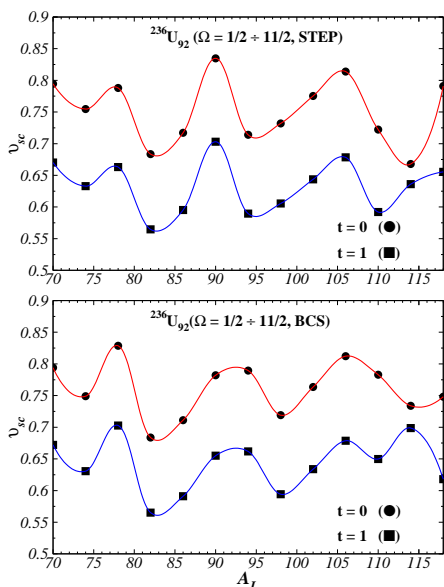

Figure 3: Scission neutron multiplicity with sudden and time-dependent approximation.
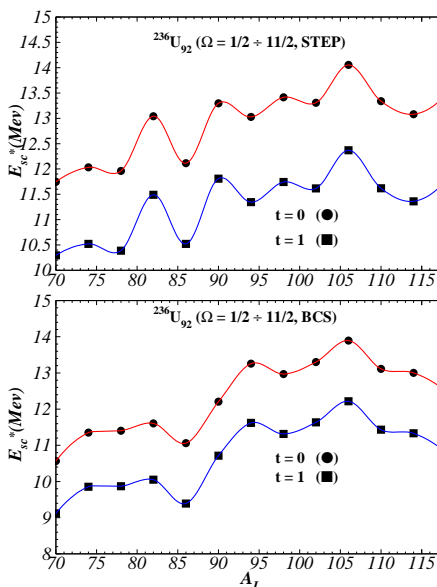

Figure 4: Primary fragments' excitation energy with sudden and time-dependent approximation.

functions obtained by diagonalization in a deformed oscillator basis, a good agreement being observed (see [8]). The finite difference approach allows however the study of a larger variety of configurations, including mass asymmetries. Both types of occupation probability calculations have been used: step function and BCS. In a previous attempt to estimate the multiplicities and the energies, we have used fixed values of probability parameters (corresponding to $A_L = 118$) for all fragment masses (see [10]). Now, we have determined these parameters for each mass ratio and we have used them in the present evaluation. This improvement produces more accurate predictions.

For each A_L we have considered several values of the projection of the total angular momentum along the symmetry axis: $\Omega = 1/2, 3/2, \cdots, 11/2$. Note that the number of bound states decreases as Ω increases. The variation of the quantities ν_{sc} and E_{sc}^* are represented in the Figs. 3 and 4 along with time-dependent results (see next section).

A direct comparison of the calculated scission-neutron multiplicity with the measurements is not possible at this moment since the separation of the scission and post-acceleration components of the prompt neutron experimental data has not been done so far. It is however interesting to note that, although the absolute values are different (the scission neutrons representing only 30% of the total prompt neutrons), the oscillations present in calculations (Fig. 3) resemble those observed experimentally [19]. The same is valid for the primary-fragments' excitation energy in Fig. 4: although it represents only a part of the total excitation energy (the other part being the extra-deformation energy), its relative variation with A_L follows roughly the experimental total excitation energy [19].

4.2 Time dependent model

An alternative approach is to consider the fission as a time dependent fast (diabatic) process. This implies the resolution of the bi-dimensional time-dependent Schrödinger equation-TDSE. The wave functions before scission are propagated during a temporal interval $[0,T]$. The potential is also time dependent, its deformation parameters changing during propagation. The moment $t=0$ corresponds to $\epsilon=0.985$, while $t=T$ corresponds to $\epsilon=1.001$. Then the propagated functions are used instead Ψ^i in the previous calculations. Thus, the physical quantities are evaluated in a more realistic model, since the scission is in reality not a sudden process, but takes some time (short but not zero).

Practically, we consider a time step Δt and advance in time a number N of steps by numerically solving at each step the time-dependent Schrödinger equation ($T = N\Delta t$). As initial solution one takes each Ψ^i. TDSE has the form

$$i\hbar \frac{\partial \Psi(\rho,z,t)}{\partial t} = \hat{\mathcal{H}}(\rho,z,t)\Psi(\rho,z,t). \tag{4.12}$$

Expanding $\hat{\mathcal{H}}$ in Taylor series with respect to t and retaining the first two terms, the formal solution of (4.12) can be written as (since only the potential V depends on t):

$$\Psi(t+\Delta t) = e^{-\frac{i}{\hbar}[\hat{\mathcal{H}}(t)\Delta t + V'(t)(\Delta t^2/2)]}\Psi(t). \tag{4.13}$$

Using the approximation $e^x \approx (1+x/2)/(1-x/2)$ (Padé of order $[1,1]$) we obtain the relation (of Crank-Nicolson type-CN):

$$\left(1 + \frac{i\Delta t}{2\hbar}\hat{\mathcal{H}} + \frac{i\Delta t^2}{4\hbar}V'\right)\Psi(t+\Delta t) = \left(1 - \frac{i\Delta t}{2\hbar}\hat{\mathcal{H}} - \frac{i\Delta t^2}{4\hbar}V'\right)\Psi(t).$$

We consider the same grid as before. Let us denote $g_{jk}^{(n)}$ the approximation of g in the point (ρ_j, z_k) and at time $t_n = n\Delta t$, where g is any of g_1 and g_2. The solution at time t_{n+1}, represented by the values $g_{jk}^{(n+1)}$, is obtained in terms of the solution at time t_n, on the basis of the above CN scheme, which turns into a linear system, after the approximation of the partial derivatives appearing in $\hat{\mathcal{H}}$ by the same finite differences formulae used in the stationary equation. The matrix of the system is typically large and sparse. The direct methods for solving (like Gauss) are inadequate, since they require too much computer memory. We have chosen an iterative method, namely the gradient method. The attractiveness of this method for large sparse systems is that it references the system matrix only through its multiplication by a vector, thus avoiding the storage of the matrix.

Given the system $\mathbf{Ax} = \mathbf{b}$ of order M, the idea is to minimize the function

$$h(\mathbf{x}) = \frac{1}{2}\mathbf{xAx} - \mathbf{bx}. \tag{4.14}$$

This function is minimized when its gradient $\nabla h = \mathbf{Ax} - \mathbf{b}$ is zero, which is equivalent to the original system. The minimization is carried out by generating a succession of vectors $\mathbf{p}_k$ and $\mathbf{x}_k$. At each stage a quantity α_k is found that minimizes $h(\mathbf{x}_k + \alpha_k \mathbf{p}_k)$ and the iteration $\mathbf{x}_{k+1}$ is set equal to $\mathbf{x}_k + \alpha_k \mathbf{p}_k$. One of the most efficient variant is the biconjugate gradient method (see [20]).

We note that the method works well for well-conditioned matrices, i.e., "close" to the identity matrix. This suggests applying this method to the preconditioned form of the equation

$$\mathbf{Ax} = \mathbf{b} : (\tilde{\mathbf{A}}^{-1}\mathbf{A})\mathbf{x} = \tilde{\mathbf{A}}^{-1}\mathbf{b}.$$

It is supposed that the system with the matrix $\tilde{\mathbf{A}}$ can be easily solved. If $\tilde{\mathbf{A}}$ is close to $\mathbf{A}$ so that $\tilde{\mathbf{A}}^{-1}\mathbf{A} \approx \mathbf{I}$ the conjugate gradient algorithm will converge fast. There are several algorithms to construct preconditioners, as the Incomplete LU Factorization and the Block Jacobi, whose description can be found in [21].

The method is applied until some convergence condition is satisfied, like

$$\frac{||\mathbf{Ax} - \mathbf{b}||}{||\mathbf{b}||} \leq \epsilon.$$

In practice we have used a subroutine based on this method adapted to complex systems (see [22]).

4.2.1 Artificial boundary conditions

To numerically solve the Schrödinger equation, the unbound physical domain should be truncated to a finite region. The conditions on the boundaries of this computational domain require a special treatment to avoid the reflexions which affect the propagated wave function and lead to errors in the calculation of the physical quantities. One possibility is to extend enough the limits of the domain and to use null values at boundaries. If the wavefunction is practically confined in a reduced area, the size of the computational domain is reasonable. Otherwise, it becomes too large and the huge number of resulting grid points generates difficulties in computer solution. Other techniques should be used in such cases, which allow reduced sizes of the numerical domain. Among them, we mention the Transparent Boundary Conditions (TBC) and the Absorbing Boundary Conditions (ABC) (see, e.g., [23–25]).

For our problem, a quite simple variant of TBC has been implemented, with satisfactory efficiency. The idea is to assume near the boundary r_B the following form of the solution: $g = g_0 \exp(ik_r r)$, where g_0 and k_r are complex constants (a 1D notation was used). Then, at the moment $t_n = n\Delta t$, we have the relations

$$\frac{g_{B+1}^n}{g_B^n} = \frac{g_B^n}{g_{B-1}^n} = \exp(ik_r \Delta r).$$

The second equality gives k_r, which is eventually adjusted so that to ensure a nonnegative flux, i.e., non radiative wave can enter in the numerical domain. The flux at the boundary has the form:

$$F(r_B) = \frac{\hbar}{m} \mathcal{R}(k_r) |g_B|^2,$$

where $\mathcal{R}$ is the real part of k_r. If $F(r_B) < 0$, $\mathcal{R}(k_r)$ is set to zero. Then g_{B+1}^n is expressed in terms of g_B^n. Supposing the same relation valid for the next time step, we obtain: $g_{B+1}^{n+1} = g_B^{n+1} \exp(ik_r \Delta r)$. These linear relations are used in the finite difference formulae for the derivatives at r_B, when the CN scheme is applied. One can see that k_r is changing as the problem progresses.

In two spatial dimensions, this algorithm should be used at each point of the grid belonging to boundaries. Of course, k_r depends on the considered point.

4.3 Time dependent approach versus sudden approximation

In the Table 4 we present scission neutron (SN) multiplicities and excitation energies (in MeV) obtained for different time intervals T at $A_L = 86$. We have used a time step $\Delta t = 1/256$ (in units of 10^{-22}s), such that $T = 1/2, 1, 4 \times 10^{-22}$s correspond respectively to $128, 256, 1024$ time steps. $T = 0$ means sudden approximation.

In order to check the convergence with respect with Δt we repeated the calculations at $A_L = 86$ and $T = 1$ using a time step 2 times smaller, i.e., $\Delta t = 1/512$. In the Table 5, we summarize the results.

Table 4: SN multiplicity and excitation energy for $A_L = 86$ at different T.

T	ν_{sc}-IP	ν_{sc}-PC	E_{sc}-IP	E_{sc}-PC
0	0.71716	0.71121	12.11418	11.05949
1/2	0.67652	0.67068	11.60120	10.54842
1	0.59526	0.59102	10.52238	9.39298
4	0.12590	0.12976	3.03274	2.07814

Table 5: Multiplicities and energies at $A_L = 86$, $T = 1$ with different Δt.

Δt	ν_{sc}-IP	ν_{sc}-PC	E_{sc}-IP	E_{sc}-PC
1/256	0.59526	0.59102	10.52238	9.39298
1/512	0.59524	0.59038	10.52308	9.41980

The agreement is quite good, especially for the Independent Particles case (the first 4 digits conserved). For this kind of nuclear calculations such an accuracy is sufficient.

In Figs. 3 and 4 we have added, respectively, the scission neutron multiplicities and the excitation energies-in MeV obtained with $N = 256$ time steps (which corresponds to $T = 1 \times 10^{-22}$ s) for $\Omega = 1/2, \cdots, 11/2$ and different $A_L \in [70, 118]$. A comparison with the sudden approximation ($N = 0, T = 0$) is thus possible.

One can see that the values of ν_{sc} and E_{sc}^* decrease when T increases (the sudden approximation is an upper limit). The results are quite relevant for the variation of these quantities with the time. The duration of the scission process is not well known. We presented data at $T = 1 \times 10^{-22}$ s for a complete set of mass asymmetries and an example of longer (4×10^{-22} s) and shorter ($1/2 \times 10^{-22}$ s) time intervals for one mass asymmetry ($A_L = 86$).

5   Conclusions

In order to numerically describe the emission of scission neutrons from fissioning nuclei we have used both the sudden approximation and a time dependent approach. This implies the solution of the bi-dimensional Schrödinger equation (BDSE), both stationary and time-dependent. Applying adequate procedures, which include Liouville transformation and special finite differences adapted to the solution behavior, we were able to determine physical quantities like neutron multiplicity and fragments' excitation energy. The neutrons were considered independent as well as pairing correlated. These two assumptions give rather close results. Of course, the occupation probabilities given by the BCS function, which takes into account the pairing correlations, are expected to be more realistic. The time-dependent approach is closer to the physical situation, but requires more calculations. If the duration of scission is short (of order $1/2 \times 10^{-22}$s) the sudden approximation is acceptable, but normally this time is longer (of order 10^{-22}s) and the

time-dependent approach should be applied. Calculations of this type for a large series of fissioning nuclei can contribute to an improved estimation and characterization of neutrons emitted during the nuclear fission. Note finally that the solution of BDSE is also of interest in other research fields, like chemical physics or laser physics.

Acknowledgments

References

[1] H. R. Bowman, S. G. Thompson, J. C. D. Milton, and W. J. Swiatecki, Velocity and angular distributions of prompt neutrons from spontaneous fission of Cf-252, Phys. Rev., 126 (1962), 2120–2136.
[2] J. K. Hwang, A. V. Ramayya, J. H. Hamilton, W. Greiner, J. D. Cole, G. M. Ter-Akopian, Yu. Ts. Oganessian, and A. V. Daniel, Search for scission neutrons in the spontaneous fission of Cf-252, Phys. Rev. C., 60 (1999), 044616.
[3] N. V. Kornilov, A. B. Kagalenko, S. V. Poupko, P. A. Androsenko, and F. J. Hambsch, New evidence of an intense scission neutron source in the Cf-252 spontaneous fission, Nucl. Phys. A., 686 (2001), 187–203.
[4] G. V. Valsky, Scission neutrons in the general systematics of the yields of light particles from ternary nuclear fission, Phys. Atom. Nucl., 67(7) (2004), 1264–1276.
[5] G. A. Petrov, Current status of the search for scission neutrons in fission and estimation of their main chracteristics, Nuclear Fission and Fission-Product Spectroscopy, AIP Conference Proceedings, 798 (2005), 205–212.
[6] G. V. Danilyan, A. V. Fedorov, V. A. Krakhotin, V. S. Pavlov, E. V. Brakhman, I. L. Karpikhin, E. Korobkina, R. Golub, T. Wilpert, and M. V. Russina, Search for scission neutrons using specific angular correlations in U-235 fission induced by slow polarized neutrons, Phys. Atom. Nucl., 69 (2006), 1158–1160.
[7] N. V. Kornilov, F. J. Hambsch, and A. S. Vorobyev, Neutron emission in fission, Nucl. Phys. A., 789 (2007), 55–72.
[8] N. Carjan, P. Talou, and O. Serot, Emission of scission neutrons in the sudden approximation, Nucl. Phys. A., 792 (2007), 102–121.
[9] Y. Boneh, and Z. Fraenkel, Dynamic single-particle effects in fission, Phys. Rev. C., 10(2) (1974), 893–900.
[10] M. Rizea, V. Ledoux, M. Van Daele, G. Vanden Berghe, and N. Carjan, Finite difference approach for the two-dimensional Schrodinger equation with application to scission-neutron emission, Comput. Phys. Commun., 179(7) (2008), 466–478.
[11] V. S. Stavinsky, N. S. Rabotnov, and A. A. Seregin, Yad. Fiz., 7 (1968), 1051 [Sov. J. Nucl. Phys., 7 (1968), 631].
[12] V. V. Pashkevich, On the asymmetric deformation of fissioning nuclei, Nucl. Phys. A., 169 (1971), 275–293.

[13] J. Damgaard, H. C. Pauli, V. V. Pashkevich, and V. M. Strutinsky, A method for solving the independent-particle Schrödinger equation with a deformed average field, Nucl. Phys. A., 135 (1969), 432–444.

[14] M. Abramowitz, and I. A. Stegun, Handbook of Mathematical Functions, 8th ed., Dover, New York, 1972.

[15] D. Sorensen, R. Lehoucq, C. Yang, and K. Maschhoff, ARPACK-An implementation of the implicitly restarted Arnoldi method for computing a few selected eigenvalues and corresponding eigenvectors of a large sparse matrix, `www.caam.rice.edu/software/ARPACK`.

[16] M. Brack, J. Damgaard, A. S. Jensen, H. C. Pauli, V. M. Strutinsky, and C. Y. Wong, Funny hills: the shell correction approach to nuclear shell effects and its applications to the fission process, Rev. Mod. Phys., 44 (1972), 320–405.

[17] P. Möller, and J. R. Nix, Nucl. Phys. A., 536 (1992), 20.

[18] A. J. Sierk, S. E. Koonin, and J. R. Nix, Modified one-body nuclear dissipation, Phys. Rev. C., 17 (1978), 646–653.

[19] K. Nishio, Y. Nakagome, H. Yamamoto, and I. Kimura, Multiplicity and energy of neutrons from $^{235}U(n_{\text{th}},f)$ fission fragments, Nucl. Phys. A., 632 (1998), 540–558.

[20] W. H. Press, S. A. Teukolsky, W. T. Vetterling, and B. P. Flannery, Numerical Recipes in Fortran-The Art of Scientific Computing, Second Edition, Cambridge University Press, 1996.

[21] G. H. Golub, and C. F. Van Loan, Matrix Computations, The Johns Hopkins University Press, 3rd Edition, 1996.

[22] H. A. van der Vorst, Bi-CGSTAB: a fast and smoothly converging variant of Bi-CG for the solution of nonsymmetric linear systems, SIAM J. Sci. Stat. Comput., 13 (1992), 631–644, `www.math.uu.nl/people/vorst/software.html`.

[23] M. Rizea, and N. Carjan, Dynamical study of proton emission from deformed nuclei, Roman. Rep. Phys., 60(1) (2008), 27–44.

[24] Z. L. Xu, H. D. Han, and X. N. Wu, Adaptive absorbing boundary conditions for Schr"odinger-type equations: application to nonlinear and multi-dimensional problems, J. Comput. Phys., 225(2) (2007), 1577–1589.

[25] X. Antoine, A. Arnold, C. Besse, M. Ehrhardt, and A. Schadle, A review of transparent and artificial boundary conditions techniques for linear and nonlinear Schrödinger equations, Commun. Comput. Phys., 4(4) (2008), 729–796.